A Comprehensive Study of Numerical Anisotropy and Dispersion in 3-D TLM Meshes

Pierre Berini, *Student Member, IEEE,* and Ke Wu, *Senior Member, IEEE*

***Abstract*—This paper presents a comprehensive analysis of the numerical anisotropy and dispersion of 3-D TLM meshes constructed using several generalized symmetrical condensed TLM nodes. The dispersion analysis is performed in isotropic lossless, isotropic lossy and anisotropic lossless media and yields a comparison of the simulation accuracy for the different TLM nodes. The effect of mesh grading on the numerical dispersion is also determined. The results compare meshes constructed with Johns' symmetrical condensed node (SCN), two hybrid symmetrical condensed nodes (HSCN) and two frequency domain symmetrical condensed nodes (FDSCN). It has been found that under certain circumstances, the time domain nodes may introduce numerical anisotropy when modelling isotropic media.**

I. Introduction

A NUMBER of generalized 3-D TLM nodes are presently capable of simulating Maxwell's curl equations in both the time and frequency domains. However, as a consequence of spatial sampling, all TLM nodes introduce numerical dispersion into the field calculations [1], [2]. Computational issues usually favor the use of one node versus another; the numerical dispersion introduced by the nodes is usually not considered due to a lack of comparative information. Furthermore, it is expected that the amount of numerical dispersion associated with a particular node may vary as a function of mesh grading and the properties of the medium modelled.

The numerical dispersion of expanded and condensed 3-D TLM meshes was originally investigated by Nielsen and Hoefer [3]–[6] where a uniform mesh is used to model free space. Their findings support the use of the condensed mesh versus the expanded mesh.

The dispersion of a 3-D frequency domain node [7] is reported in [8] where the mesh grading and the properties of the medium are varied. A significant difference was observed between the dispersion characteristics of the graded and uniform meshes in [8]. As pointed out by our reviewers, a dispersion analysis of time and frequency domain meshes was recently reported by the same authors [9]. We cannot comment on the contents of this paper as it was inaccessible at the time of publication.

Section II of this paper includes a brief review of the numerical dispersion relation originally derived by Nielsen and Hoefer [3], [4]. A more general formulation of this method is presented such that the dispersion analysis may be carried out in anisotropic and lossy media using any 3-D TLM node. In Section III, the dispersion characteristics of various 3-D TLM meshes are given for different modelling requirements. Five 3-D SCN's are used; they include three time domain nodes: Johns' SCN [10]–[13], the type I HSCN [14]–[16] and the type II HSCN [16]. Two frequency domain nodes are also included: the type I FDSCN [7], [17]–[19] and the type II FDSCN [19], [20]. The above nodes share the common characteristics of being symmetrical, condensed and reasonably general; the type I FDSCN, however, cannot model material anisotropy.

Manuscript received April 5, 1994; revised September 27, 1994. This work was supported by NSERC and FCAR.

The authors are with the Groupe de Recherches avancées en Microondes et Électronique Spatiale (POLY-GRAMES), Département de Génie Électrique et Informatique, École Polytechnique de Montréal, Montréal, Québec, Canada H3C 3A7.

IEEE Log Number 9410343.

II. Formulation

A. Generalized Numerical Dispersion Relation

The analysis technique for numerical dispersion described in [4] consists in computing the propagation constant of an arbitrary plane wave propagating on an infinite homogeneous mesh constructed from identical 3-D TLM nodes. This is achieved by solving the following determinantal equation:

$$|PQ - W| = 0 \tag{1}$$

where

$$Q = (I + S_n)T \tag{2}$$

and

$$W = I + TS_nT. \tag{3}$$

$[I]_{(12\times12)}$ is the identity matrix. S_n is the frequency domain scattering matrix of the node used to create the mesh and is defined at the center of the node, not at the input/output plane of the link lines.

The propagation matrix T represents the connection between nodes and has the following non-zero elements:

$$\begin{aligned} T_{1,1} &= T_{12,12} = e^{-\gamma_{yx}\Delta_y} \\ T_{2,2} &= T_{9,9} = e^{-\gamma_{zx}\Delta_z} \\ T_{3,3} &= T_{11,11} = e^{-\gamma_{xy}\Delta_x} \\ T_{4,4} &= T_{8,8} = e^{-\gamma_{zy}\Delta_z} \\ T_{5,5} &= T_{7,7} = e^{-\gamma_{yz}\Delta_y} \\ T_{6,6} &= T_{10,10} = e^{-\gamma_{xz}\Delta_x}. \end{aligned} \tag{4}$$

The propagation constants γ_{ij} are associated with the link lines according to Fig. 1. The subscripts ij indicate the direction of propagation and the polarization, respectively, of the associated voltage wave. This definition of matrix T is necessary

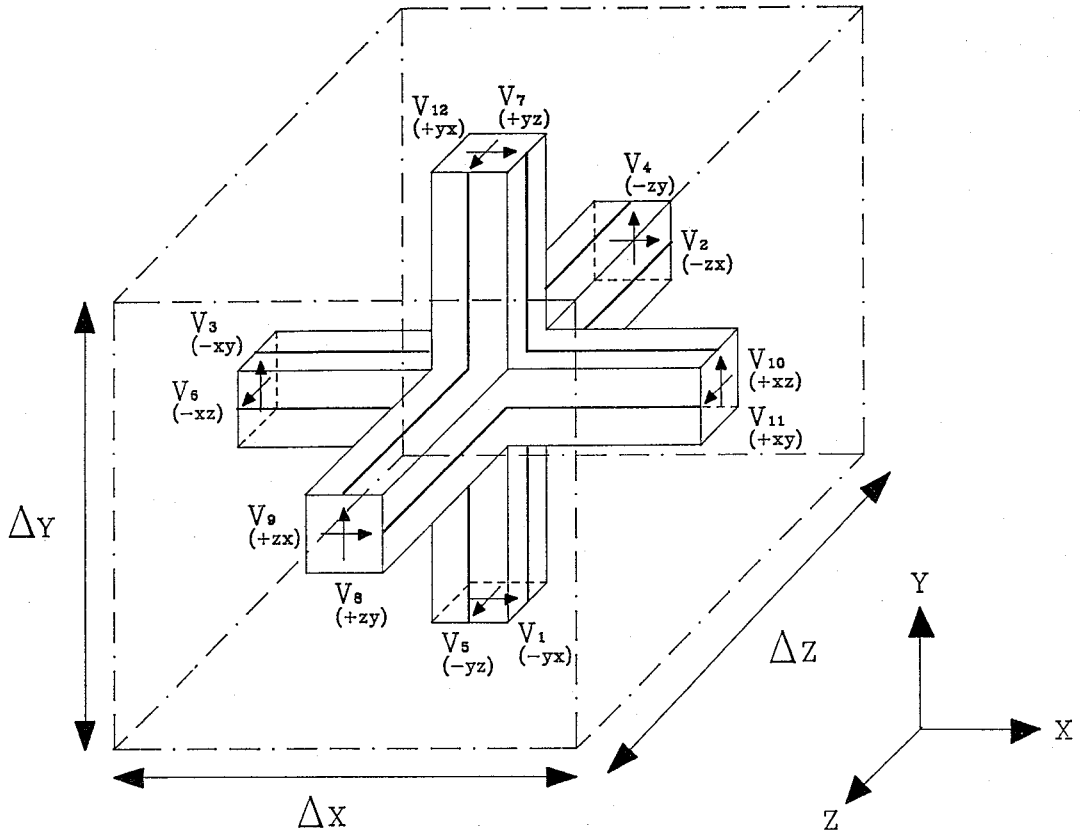

Fig. 1. TLM Symmetrical Condensed Node.

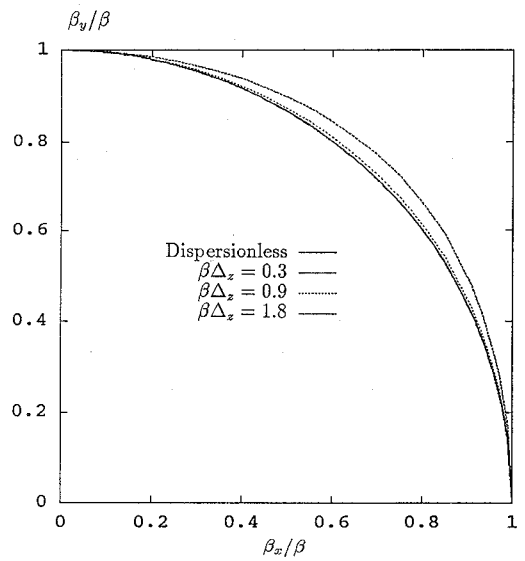

Fig. 2. Dispersion characteristics of case study given in Table I.

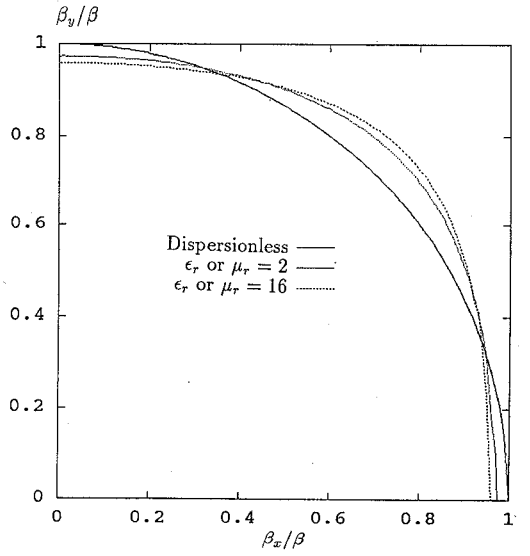

Fig. 3. Dispersion characteristics of case study given in Table I. $\beta\Delta_z = 1.8$ throughout.

to accommodate nodes that vary the propagation constant of the link lines to model certain properties of the medium or to account for a graded mesh.

Matrix P represents Floquet's theorem, relating the total voltages at one node to the total voltages at the neighboring nodes along this periodic network. The superscript m denotes the *mesh* propagation constants

$$P_{1,12} = e^{\gamma^m_{yx}\Delta_y}, \quad P_{12,1} = e^{-\gamma^m_{yx}\Delta_y}$$
$$P_{2,9} = e^{\gamma^m_{zx}\Delta_z}, \quad P_{9,2} = e^{-\gamma^m_{zx}\Delta_z}$$
$$P_{3,11} = e^{\gamma^m_{xy}\Delta_x}, \quad P_{11,3} = e^{-\gamma^m_{xy}\Delta_x}$$
$$P_{4,8} = e^{\gamma^m_{zy}\Delta_z}, \quad P_{8,4} = e^{-\gamma^m_{zy}\Delta_z}$$
$$P_{5,7} = e^{\gamma^m_{yz}\Delta_y}, \quad P_{7,5} = e^{-\gamma^m_{yz}\Delta_y}$$
$$P_{6,10} = e^{\gamma^m_{xz}\Delta_x}, \quad P_{10,6} = e^{-\gamma^m_{xz}\Delta_x}. \tag{5}$$

This new definition of matrix P allows the determination of the numerical dispersion characteristics in lossy and anisotropic media.

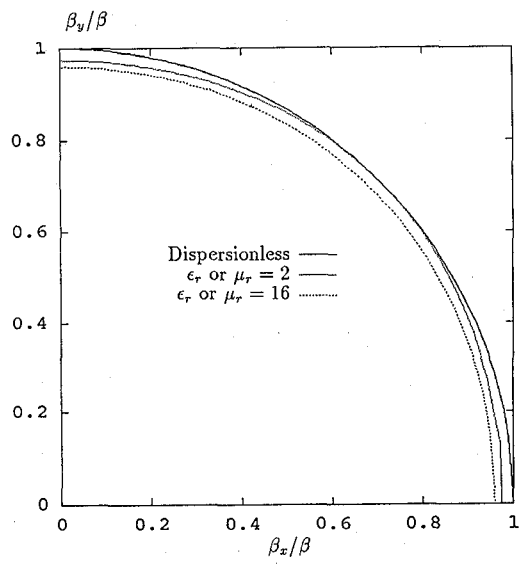

Fig. 4. Dispersion characteristics of case study given in Table I. $\beta\Delta_z = 1.8$ throughout.

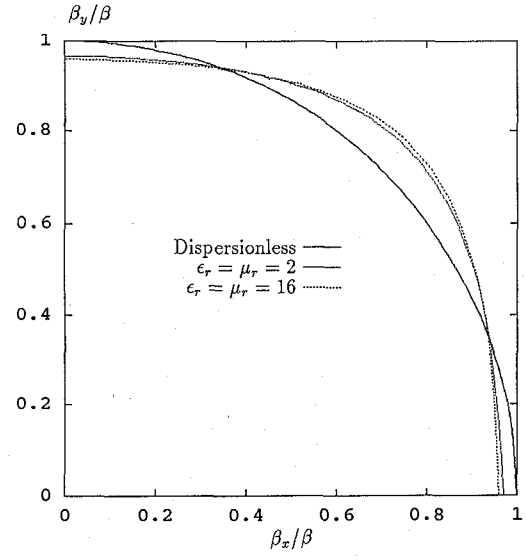

Fig. 5. Dispersion characteristics of case study given in Table I. $\beta\Delta_z = 1.8$ throughout.

The dispersion of a mesh is obtained by solving numerically the determinantal equation (1) for the mesh propagation constant of an arbitrary plane wave. In practice, this can be achieved by finding the values γ_{ij}^m that minimise the absolute value of the determinant in (1) for a given wave orientation.

It must be noted that the formulation of the dispersion relation given in [3] is numerically equivalent to (1).

B. Transformation of a Time Domain Node to the Frequency Domain

The dispersion analysis of a TLM mesh is carried out in the frequency domain. Furthermore, the scattering event does not occur but is implied through the use of the frequency domain voltage scattering matrix S_n and the transmission matrix T defined above. If a generalized time domain node is used to create the mesh then this node must be transformed to an equivalent frequency domain node. This is accomplished by

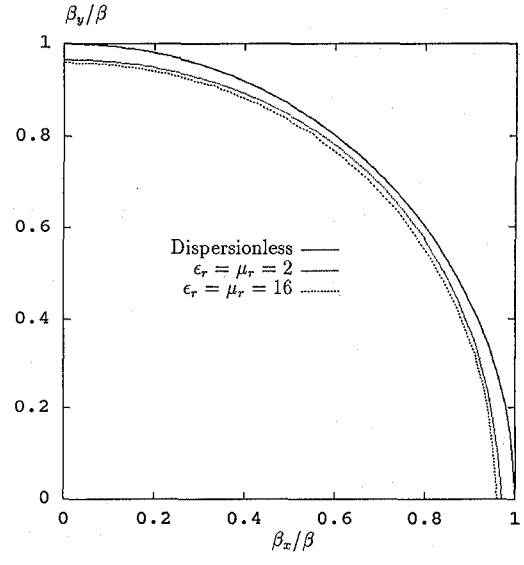

Fig. 6. Dispersion characteristics of case study given in Table I. $\beta\Delta_z = 1.8$ throughout.

TABLE I
CASE STUDY OF LOSSLESS ISOTROPIC MEDIA MODELLED USING A UNIFORM MESH. FIGURE CROSS-REFERENCING. VER: VERTICAL POLARIZATION, HOR: HORIZONTAL POLARIZATION

Medium		SCN		HSCN I		HSCN II	
ϵ_r	μ_r	Ver	Hor	Ver	Hor	Ver	Hor
1	1	2	2	2	2	2	2
2	1	4	3	4	3	3	4
16	1	4	3	4	3	3	4
1	2	3	4	4	3	3	4
1	16	3	4	4	3	3	4
2	2	2	2	6	5	5	6
16	16	2	2	6	5	5	6

treating the voltage impulses as complex voltage waves and by absorbing the stubs into an equivalent 12×12 stubless matrix, according to basic S matrix theory.

Consider for example the 18×18 voltage scattering matrix of an arbitrary time domain SCN, loaded with both open and short circuit stubs. This matrix can be decomposed into four submatrices as follows [18]:

$$\begin{bmatrix} \boldsymbol{V}_m^r \\ \boldsymbol{V}_s^r \end{bmatrix} = \begin{bmatrix} [S_{mm}]_{(12\times12)} & [S_{ms}]_{(12\times6)} \\ [S_{sm}]_{(6\times12)} & [S_{ss}]_{(6\times6)} \end{bmatrix} \begin{bmatrix} \boldsymbol{V}_m^i \\ \boldsymbol{V}_s^i \end{bmatrix} \tag{6}$$

where the subscript m refers to the 12 mesh lines and s refers to the 6 possible open and short circuit stubs. In the frequency domain, the relationship between the voltage waves incident to and reflected from the stubs is written

$$\boldsymbol{V}_s^i = [\Gamma_s]_{\text{diag}} e^{-j\theta_s} \boldsymbol{V}_s^r \tag{7}$$

where $[\Gamma_s]_{\text{diag}}$ is a diagonal matrix constructed from the reflection coefficient of the stubs and θ_s refers to the phase shift encountered by a voltage wave during the return trip through a stub. The matrix $[\Gamma_s]_{\text{diag}}$ is defined as

$$\begin{aligned} \Gamma_{i,i} &= +1, \quad \text{for } i = 1,2,3 \\ \Gamma_{i,i} &= -1, \quad \text{for } i = 4,5,6. \end{aligned} \tag{8}$$

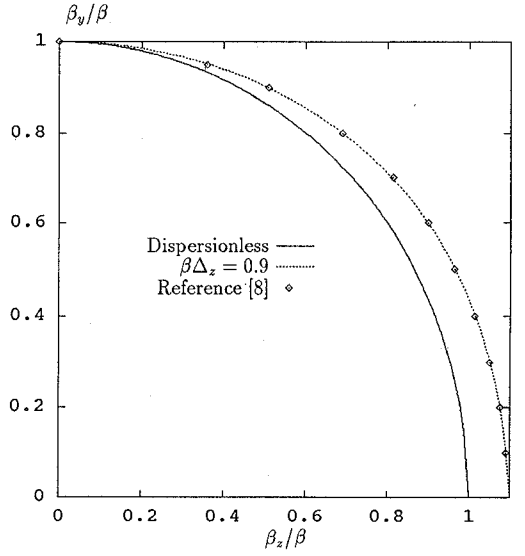

Fig. 7. Dispersion characteristics of a graded mesh modelling free space and constructed with type I FDSCN's. Cell dimensions: $\Delta_x = \Delta_z = 10$ cm and $\Delta_y = 5$ cm.

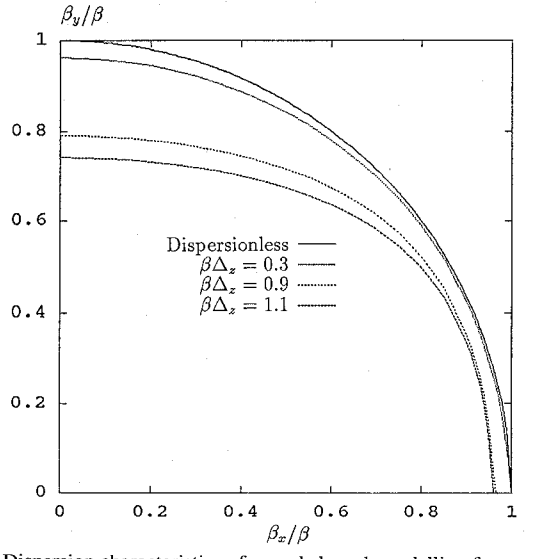

Fig. 8. Dispersion characteristics of a graded mesh modelling free space and constructed with SCN's. Cell dimensions; $\Delta_x = 10$ cm, $\Delta_y = 15$ cm, and $\Delta_z = 5$ cm.

Using the above equations, we can reduce the original 18×18 time domain scattering matrix to an equivalent stubless 12×12 frequency domain scattering matrix S_n

$$\boldsymbol{V}_m^r = [S_n]\boldsymbol{V}_m^i \tag{9}$$

where

$$S_n = S_{mm} + S_{ms}\overbrace{(e^{j\theta_s}[\Gamma_s] - S_{ss})^{-1}}^{\text{diagonal}} S_{sm} \tag{10}$$

which is similar to the result given in [18]. The reference plane can be moved from the center of the node to the input/output port of the link lines by multiplying $[S_n]$ with $e^{-j\theta_s}$. The matrix S_n defined by (10) can be used directly in (2) and (3) and the elements of T are $T_{i,i} = e^{-j\theta_s}$.

Johns' symmetrical condensed node: We can directly identify the submatrices $[S_{mm}]_{12\times12}$, $[S_{ms}]_{12\times6}$, $[S_{sm}]_{6\times12}$ and $[S_{ss}]_{6\times6}$ for Johns' SCN [10]–[13]. The lower 6×18 sub-

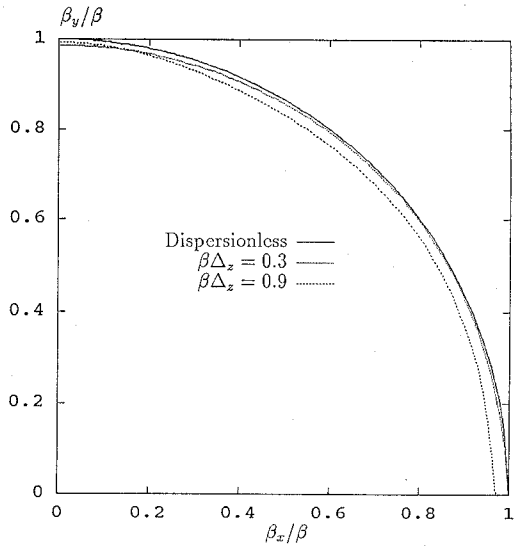

Fig. 9. Dispersion characteristics of a graded mesh modelling free space and constructed with HSCN's; vertical pol.: HSCN I and horizontal pol.: HSCN II. Cell dimensions: $\Delta_x = 10$ cm, $\Delta_y = 15$cm, and $\Delta_z = 5$ cm.

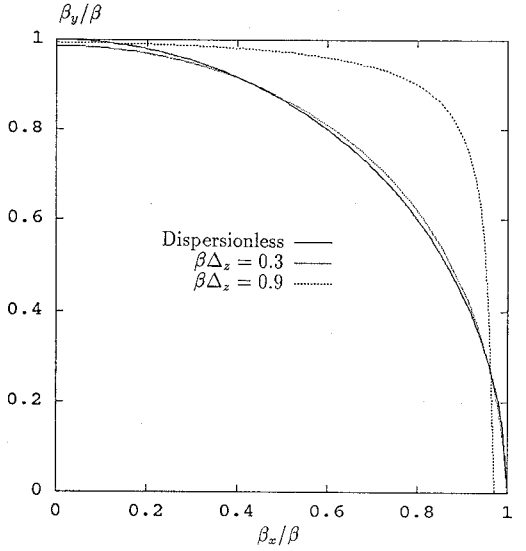

Fig. 10. Dispersion characteristics of a graded mesh modelling free space and constructed with HSCN's; vertical pol.: HSCN II and horizontal pol.: HSCN I. Cell dimensions: $\Delta_x = 10$ cm, $\Delta_y = 15$ cm, and $\Delta_z = 5$ cm.

matrix represents scattering into the matched loss stubs; it is not included in the frequency domain matrix as these stubs do not return their impulses to the node. The time step Δ_t is chosen in the usual manner as the largest possible value that ensures positive characteristic impedances for the permittivity and permeability stubs. The phase shift θ_s is defined for Johns' SCN as $\theta_s = \omega\Delta_t$.

Hybrid symmetrical condensed nodes: Both hybrid nodes given in [16] can be transformed to the frequency domain using (8) and (10) directly. It must be noted that the hybrid nodes are described using an 18×18 scattering matrix with appropriate null elements [16]. This contrasts with the alternate description of the HSCN found in [14]. For both types of HSCN's, the phase shift θ_s is defined as $\theta_s = \beta_0\Delta_l/2$ where $\beta_0 = \omega/c_0$ and $c_0 = 1/\sqrt{\epsilon_0\mu_0}$. This is the same phase shift

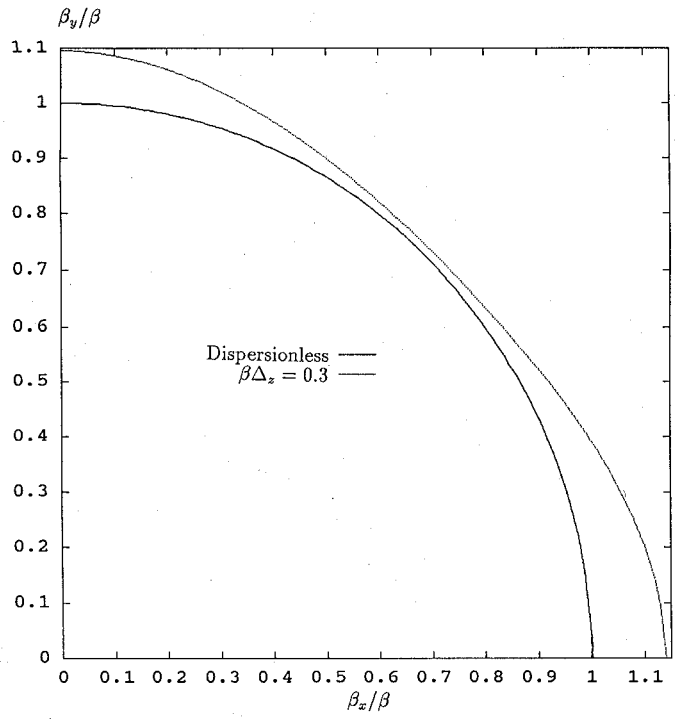

Fig. 11. Dispersion characteristics of a graded mesh constructed with type I FDSCN's. Cell dimensions: $\Delta_x = 10$ cm, $\Delta_y = 15$ cm, and $\Delta_z = 5$ cm.

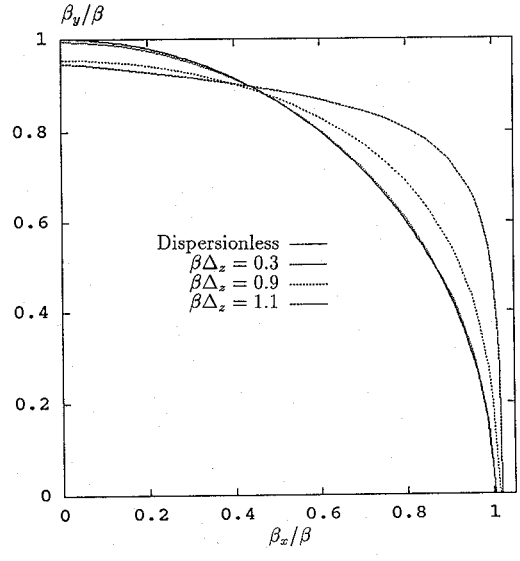

Fig. 12. Dispersion characteristics of a graded mesh constructed with type II FDSCN's. Cell dimensions: $\Delta_x = 10$ cm, $\Delta_y = 15$ cm, and $\Delta_z = 5$ cm.

as in Johns' SCN since the time step for the hybrid nodes is taken as $\Delta_t = \Delta_l/(2c_0)$.

Frequency domain symmetrical condensed nodes: Both SCN's derived in the frequency domain [7], [19] can be used without modification in the dispersion analysis. The scattering matrix S_v and the propagation constant of the link lines defined in [7], [19] are used directly in (2)–(4).

III. Numerical Results and Discussion

The dispersion characteristics given in this section are obtained using the technique presented above. In part A, lossless isotropic media is considered; in part B, the mesh grading is varied; in part C, lossy isotropic media is modelled and in part D, lossless anisotropic media. In all cases vertically and horizontally polarized plane waves are swept through all angles in the plane considered. Generally three frequencies are analysed in order to vary the coarseness of the mesh.

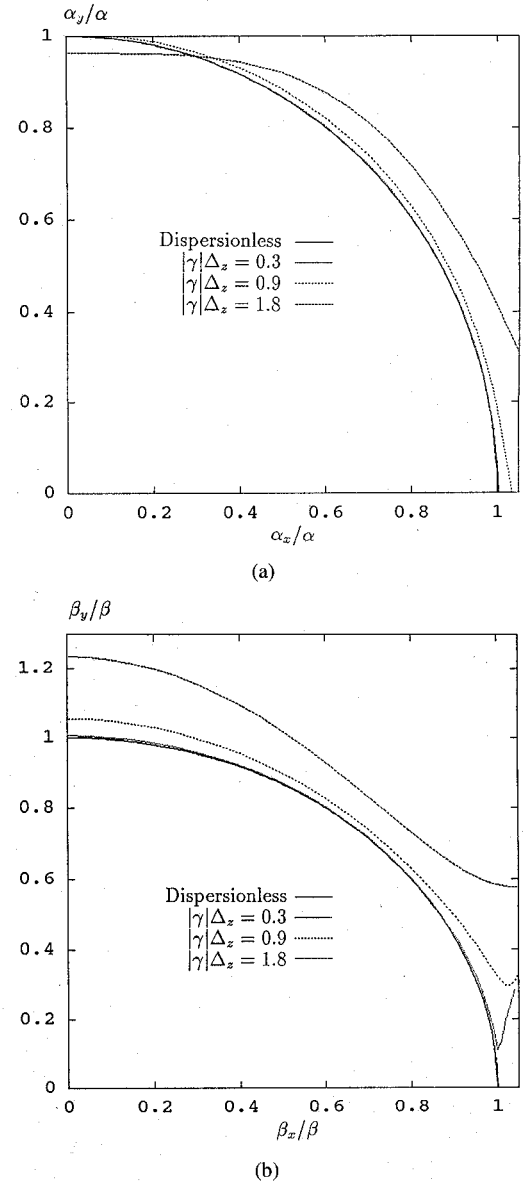

Fig. 13. Dispersion characteristics of a uniform mesh constructed with SCN's and modelling a lossy isotropic medium characterized by $\epsilon_r = \mu_r = 5\text{-}j5$. (a) Normalized attenuation constant. (b) Normalized phase constant.

A. Lossless Isotropic Media

The permittivity and permeability of the medium are varied in order to observe changes in the dispersion characteristics of the homogeneous meshes created using the five nodes described above. A uniform mesh, $\Delta_x = \Delta_y = \Delta_z = 5$ cm, is used to generate Figs. 2–6. The phase constant β is that of a plane wave propagating in the medium considered.

The first medium modelled is free space. This is a natural starting point as all nodes considered, reduce in this case, to the same node in the frequency domain. Fig. 2 gives the

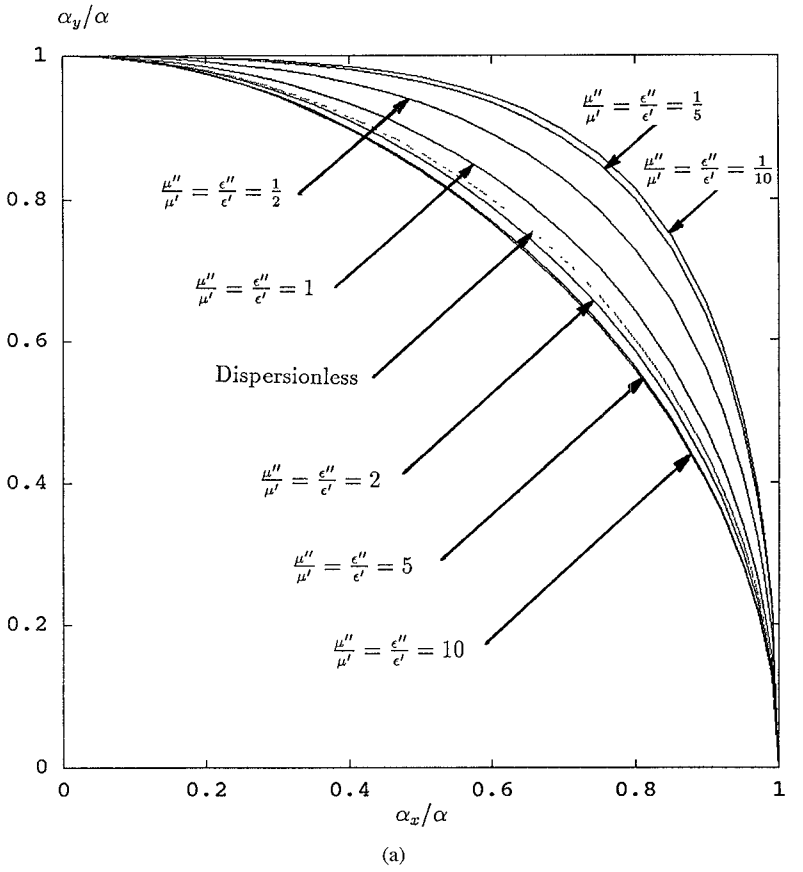

(a)

Fig. 14. Dispersion characteristics of a uniform mesh modelling various lossy isotropic media and constructed with FDSCN's. (a) Normalized attenuation constant. $|\gamma|\Delta_z = 1.8$ throughout.

free space dispersion characteristics; the results are identical to those given in [4] and [8].

The dispersion characteristics of the FDSCN mesh remain identical to those given in Fig. 2, regardless of the permittivity or permeability of the medium. Two cases were analysed to confirm this, the first $\epsilon_r = 4$, $\mu_r = 1$ and the second $\epsilon_r = 25$, $\mu_r = 20$. This observation is consistent with the results given in [8]. It must be noted that if the mesh is uniform and the medium considered is isotropic, both FDSCN's are in fact the same node.

The various media modelled using the time domain nodes are summarized in Table I where they are cross-referenced with the appropriate figures. For example, according to Table I, Fig. 4 gives the dispersion characteristics for the vertical polarization of a plane wave propagating in a medium characterized by $\epsilon_r = 2$ and $\mu_r = 1$ and modelled with a SCN mesh.

From Figs. 3–6 we observe that the time domain nodes introduce anisotropy into the dispersion characteristics when the permittivity or permeability of the medium differs from free space. Anisotropy is observed when the phase constant of a vertically polarized wave differs from that of a horizontally polarized wave. If a wave propagates in the xy plane, the electric field of the vertically polarized wave will be directed along the z axis whereas the electric field of the horizontally polarized wave will be in the xy plane.

The dispersion characteristics of the SCN mesh are identical to the type I HSCN mesh if $\mu_r = 1$ or to the type II HSCN mesh if $\epsilon_r = 1$; this is expected when a uniform mesh is used, as the HSCN's are identical to the SCN in those circumstances. It is interesting to note that the dispersion characteristics of the meshes constructed with HSCN's are complementary; that is, the dispersion of the vertical polarization of an HSCN I mesh is identical to the dispersion of the horizontal polarization of an HSCN II mesh and vice versa. For the special case where $\epsilon_r = \mu_r \geq 1$ the dispersion characteristics for the SCN remain identical to those given in Fig. 2. We note that the time domain meshes are isotropic for the limiting case of axial propagation. The anisotropy introduced by the time domain nodes are responsible for the separation of the degenerate TE/TM11 and TE/TM21 modes of the rectangular waveguide analysed in [19].

B. Grading

The effect of grading on the dispersion characteristics of the five meshes is investigated. In Figs. 7–12, the phase constant β is that of a plane wave propagating in the medium considered. In all cases the analysis frequency was increased until (1) could no longer be easily minimized.

Fig. 7 illustrates the dispersion characteristics of a plane wave propagating in free space. The graded mesh is constructed using the type I FDSCN and the cell dimensions are

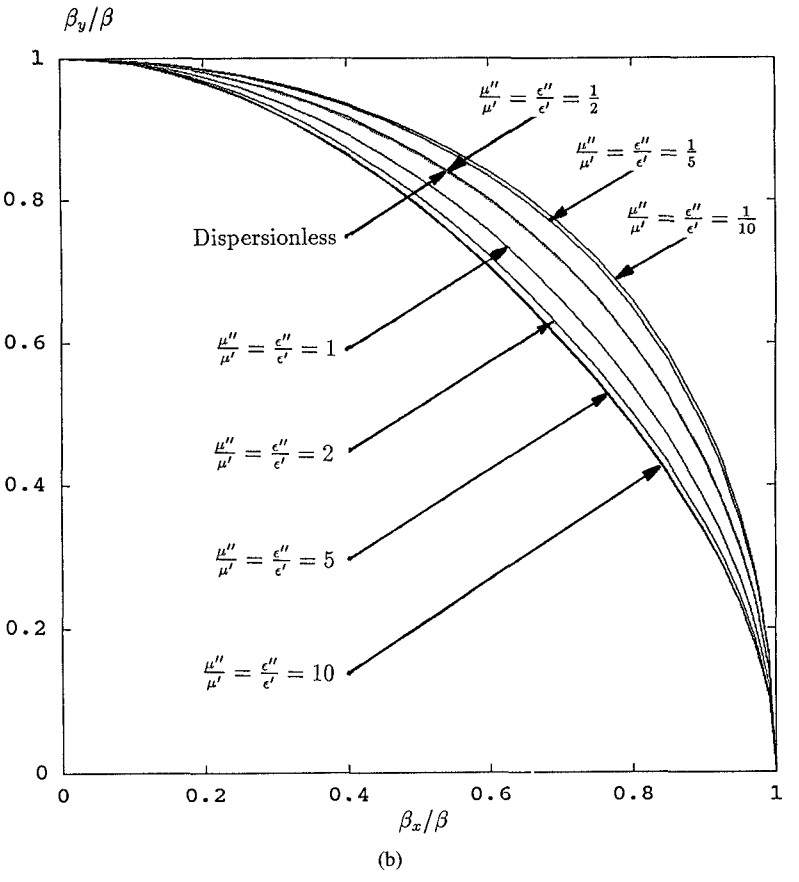

(b)

Fig. 14. (continued) (b) Normalized phase constant.

$\Delta_x = \Delta_z = 10$ cm and $\Delta_y = 5$ cm. Perfect agreement is observed with the results given in [8].

Figs. 8–12 display the dispersion characteristics of a plane wave propagating in the xy plane. A graded mesh of dimensions $\Delta_x = 10$ cm, $\Delta_y = 15$ cm, and $\Delta_z = 5$ cm is used. The time domain meshes model free space.

Both HSCN's introduce anisotropy when a graded mesh is used. Fig. 9 gives the dispersion characteristics of the vertically polarized wave on the type I HSCN mesh and of the horizontally polarized wave on the type II HSCN mesh; Fig. 10 shows the dispersion characteristics of the vertically polarized wave on the type II HSCN mesh and of the horizontally polarized wave on the type I HSCN mesh. Once again, the dispersion characteristics of the HSCN meshes are complementary. For the limiting case of axial propagation, the HSCN meshes are isotropic. By comparing Fig. 8 with Figs. 9 and 10 we note that the HSCN meshes introduce less dispersion than the SCN mesh along a principal axis. This observation is consistent with the results given in [14].

The dispersion characteristics plotted in Figs. 11 and 12, obtained using the frequency domain nodes, were found to be invariant regardless of the permittivity and permeability of the medium; this is consistent with the observations made in the preceeding section. Such an invariance however, should not be expected from the time domain nodes except perhaps for the SCN if $\epsilon_r = \mu_r$.

It is observed, by comparing Fig. 9 with Figs. 8, 11, and 12, that one of the polarizations supported by an HSCN mesh suffers much less numerical dispersion. This suggests that even though the HSCN's introduce numerical anisotropy, they may yet model more accurately certain electromagnetic modes on a graded mesh.

C. Lossy Isotropic Media

Complex permittivities and permeabilities are now introduced in order to observe changes in the dispersion characteristics of the meshes for lossy media. A uniform mesh, $\Delta_x = \Delta_y = \Delta_z = 5$ cm, is used to generate Figs. 13 and 14. The propagation constant $\gamma = \alpha + j\beta$ is that of a plane wave propagating in the medium considered.

Fig. 13 gives the dispersion curves of an SCN mesh modelling a lossy medium characterized by $\epsilon_r = \mu_r = 5\text{-}j5$. Once again, we note that in this special case, the node does not introduce anisotropy.

The dispersion characteristics for a mesh constructed with HSCN's are difficult to obtain in lossy media due to the anisotropy that is introduced; (1) cannot easily be minimized. It can however be said that they are complementary and that the horizontal polarization for a type I HSCN mesh and the vertical polarization for a type II HSCN mesh are similar, though more dispersive, than the characteristics shown in Fig. 13.

The dispersion characteristics of a mesh constructed with FDSCN's are, in contrast to time domain nodes, quite easy to obtain; a more thorough case study is thus given in Fig. 14. Contrary to the observations made in Section I, the dispersion characteristics of meshes constructed with FDSCN's are found

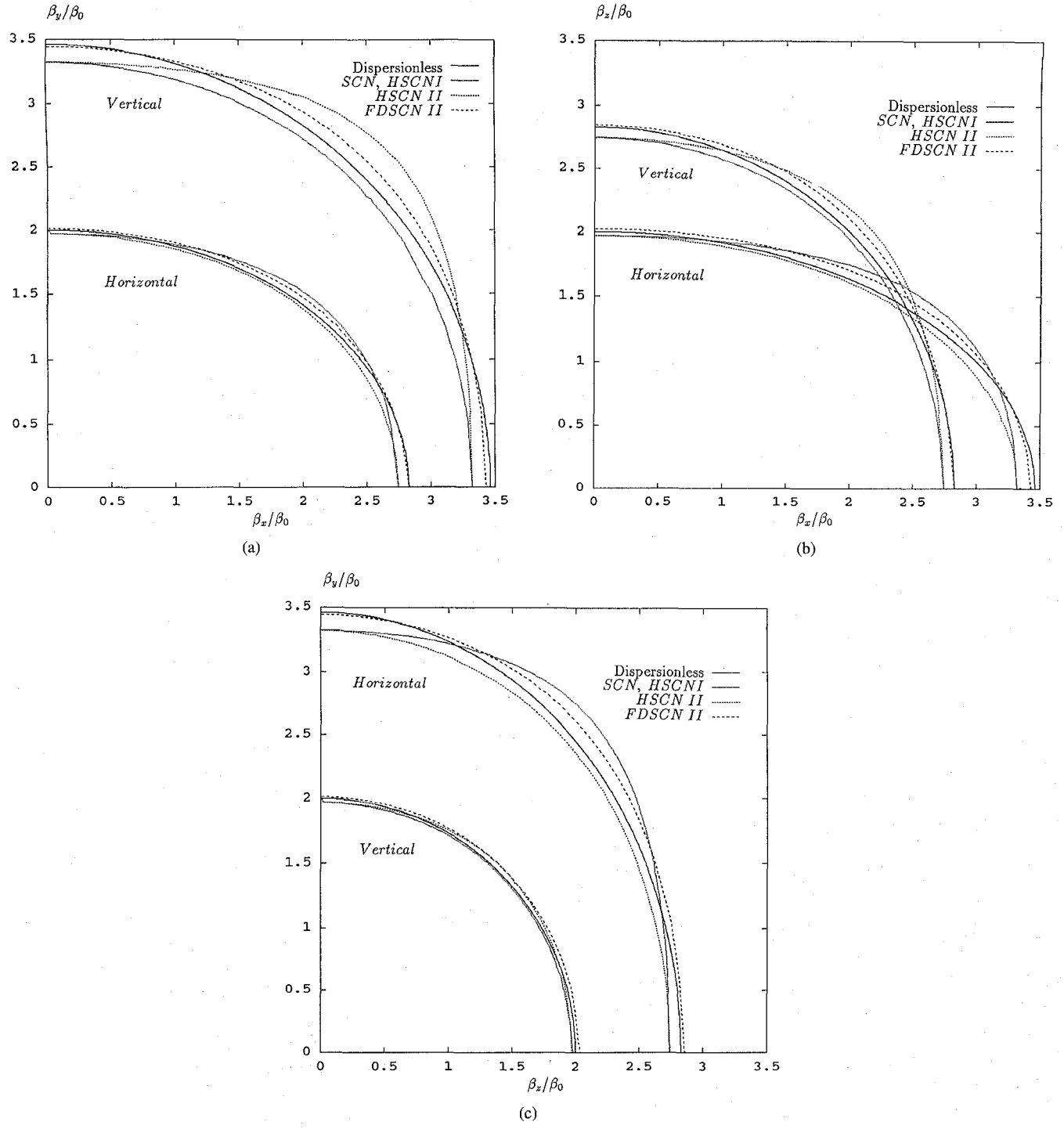

Fig. 15. Dispersion characteristics of a uniform mesh constructed with various SCN's and modelling an anisotropic lossless medium characterized by $\epsilon_{xx,r} = 4$, $\epsilon_{yy,r} = 8$ and $\epsilon_{zz,r} = 12$. (a) xy plane. (b) xz plane. (c) zy plane. $\beta\Delta_z = 1.8$ throughout.

to vary in lossy media. They are however only sensitive to the ratios $\epsilon''/\epsilon', \mu''/\mu'$ and not to the actual values of permittivity and permeability.

D. Lossless Anisotropic Media

A lossless anisotropic medium described by a diagonal permittivity tensor is now considered. In a biaxial medium, the velocity of a plane wave is dependent on the orientation of its wave normal. In general, there can exist only two forward and two backward propagating waves for each direction of wave normal. The two forward propagating waves for example, correspond to the two eigenwaves or polarizations permitted by the medium for the given wave normal. The velocity of these eigenwaves are obtained from Fresnel's equation of wave normals [21], [22]

$$b_x^2(v_{yy}^2 - v_p^2)(v_{zz}^2 - v_p^2) + b_y^2(v_{xx}^2 - v_p^2)(v_{zz}^2 - v_p^2) + b_z^2(v_{xx}^2 - v_p^2)(v_{yy}^2 - v_p^2) = 0 \quad (11)$$

where v_p is the velocity of the eigenwaves and b_x, b_y and b_z are the components of the unit vector normal to the wave,

defined as

$$\hat{\boldsymbol{b}} \| \boldsymbol{D} \times \boldsymbol{H} \tag{12}$$

$\boldsymbol{D}$ is the electric flux density and $\boldsymbol{H}$ the magnetic field intensity. v_{xx}, v_{yy} and v_{zz} are the wave velocities along the principal axes

$$v_{xx} = \frac{c_0}{\sqrt{\epsilon_{xx,r}\mu_r}},\ v_{yy} = \frac{c_0}{\sqrt{\epsilon_{yy,r}\mu_r}},\ v_{zz} = \frac{c_0}{\sqrt{\epsilon_{zz,r}\mu_r}} \tag{13}$$

where $c_0 = 1/\sqrt{\epsilon_0\mu_0}$. Fresnel's equation of wave normals is a quadratic equation in v_p^2 that can be solved analytically. Two solutions for v_p^2 are obtained; they correspond to the two allowed polarizations associated with the given wave normal. The two roots of v_p^2 correspond to the forward and backward travelling waves, thus four velocities are obtained per wave normal. Equation (11) is solved in order to generate the theoretical *dispersionless* curves presented in this section.

Fig. 15 compares the dispersion characteristics of four uniform meshes, $\Delta_x = \Delta_y = \Delta_z = 5$ cm, in a medium characterized by $\epsilon_{xx,r} = 4$, $\epsilon_{yy,r} = 8$ and $\epsilon_{zz,r} = 12$. The type I FDSCN is not included in these results as it cannot model anisotropy. The frequency of analysis is chosen such that $\beta\Delta_z = 1.8$ where β is the phase constant of a plane wave propagating in an isotropic medium having $\epsilon_r = 12$.

IV. Conclusion

A thorough study of the numerical dispersion of various 3-D TLM meshes has been presented. Five symmetrical condensed nodes including three time domain and two frequency domain nodes were used to construct the meshes. The dispersion characteristics were obtained in lossless isotropic, lossy isotropic and lossless anisotropic media. The effect of mesh grading has also been investigated.

The results obtained reveal that under certain circumstances, the time domain nodes introduce anisotropy into the dispersion characteristics of isotropic media. It also appears that the ability of the time domain nodes to simulate lossy media is limited to the case where the losses are small. The most significant degradation of the dispersion characteristics, however, occur when a coarse graded mesh is used, indicating that the largest cell dimension should be much smaller than the smallest wavelength under consideration.

The best way to improve TLM simulation accuracy is of course mesh refinement. The results presented in this paper, however, are of particular importance if a coarse mesh must be used as the numerical dispersion and anisotropy introduced may significantly corrupt the field calculations. In such a case, these results may be used as an aid in the selection of the node best suited to specific modelling requirements.

References

[1] W. J. R. Hoefer, "The transmission-line matrix method—Theory and applications," *IEEE Trans. Microwave Theory Tech.*, vol. MTT-33, pp. 882–893, Oct. 1985.

[2] ——, "The transmission line matrix (TLM) method," in *Numerical Techniques for Microwave and Millimeter-Wave Passive Structures*. New York: Wiley Interscience, 1989.

[3] J. Nielsen, "Spurious modes of the TLM-condensed node formulation," *IEEE Microwave and Guided Wave Lett.*, vol. 1, pp. 201–203, Aug. 1991.

[4] J. Nielsen and W. Hoefer, "A complete dispersion analysis of the condensed node TLM mesh," *IEEE Trans. Magn.*, vol. 27, pp. 3982–3985, Sept. 1991.

[5] ——, "Effect of dispersion in the 3-D condensed node TLM mesh," in *IEEE MTT-S Int. Microwave Symp. Dig.*, 1992, pp. 853–855.

[6] ——, "Generalized dispersion analysis and spurious modes of 2-D and 3-D TLM formulations," *IEEE Trans. Microwave Theory Tech.*, vol. 11, pp. 1375–1384, Aug. 1993.

[7] D. P. Johns, A. J. Wlodarczyk, A. Mallik, and C. Christopoulos, "New TLM technique for steady—State field solutions in three dimensions," *Electron. Lett.*, vol. 28, pp. 1692–1694, Aug. 1992.

[8] D. P. Johns and C. Christopoulos, "Dispersion characteristics of 3-D frequency-domain TLM," *Electron. Lett.*, vol. 29, pp. 1536–1537, Aug. 1993.

[9] ——, "Dispersion of time-domain and frequency-domain formulations of the symmetrical condensed TLM node," in *Proc. 2nd Int. Conf. Computations in Electromagn.*, pub. 384, 1994, pp. 295–298.

[10] P. B. Johns, "A symmetrical condensed node for the TLM method," *IEEE Trans. Microwave Theory Tech.*, vol. MTT-35, pp. 370–377, Apr. 1987.

[11] ——, "Use of condensed and symmetrical TLM nodes in computer-aided electromagnetic design," *IEE Proc.*, pt. H, vol. 133, pp. 368–374, Oct. 1986.

[12] P. Naylor and R. A. Desai, "New three dimensional symmetrical condensed node for solution of electromagnetic wave problems by TLM," *Electron. Lett.*, vol. 26, pp. 492–494, Mar. 1990.

[13] F. J. German, G. K. Gothard, and L. S. Riggs, "Modelling of materals with electric and magnetic losses with the symmetrical condensed TLM method," *Electron. Lett.*, vol. 26, pp. 1307–1308, Aug. 1990.

[14] R. Scaramuzza and A. J. Lowery, "Hybrid symmetrical condensed node for the TLM method," *Electron. Lett.*, vol. 28, pp. 1947–1949, Nov. 1990.

[15] R. Scaramuzza, P. Naylor, and C. Christopoulos, "Numerical simulation of field-to-wire coupling using transmission line modelling," in *Int. Conf. Computations in Electromagn.*, pub. 350, pp. 63–66, 1991.

[16] P. Berini and K. Wu, "A pair of hybrid symmetrical condensed TLM nodes," *IEEE Microwave and Guided Wave Lett.*, vol. 4, pp. 244–246, July 1994.

[17] J. Huang, R. Vahldieck, and H. Jin, "Fast frequency-domain TLM analysis of 3D circuit discontinuities," in *Proc. 9th Annual Rev. Progress in Applied Computational Electromagn. Symp.*, 1993, pp. 475–480.

[18] H. Jin, R. Vahldieck, J. Huang, and P. Russer, "Rigorous analysis of mixed transmission line interconnects using the frequency-domain TLM method," *IEEE Trans. Microwave Theory Tech.*, vol. MTT-41, pp. 2248–2255, Dec. 1993.

[19] P. Berini and K. Wu, "A new frequency domain symmetrical condensed TLM node," *IEEE Microwave and Guided Wave Lett.*, vol. 4, pp. 180–182, June 1994.

[20] D. P. Johns, "Improved node for frequency-domain TLM: The 'distributed node'," *Electron. Lett.*, vol. 30, pp. 500–502, Mar. 1993.

[21] A. Yariv and Y. Pochi, *Optical Waves in Crystals, Propagation and Control of Laser Radiation*. New York: Wiley Interscience, 1984.

[22] J. F. Nye, *Physical Properties of Crystals*. London: Oxford University Press, 1957.

Pierre Berini (S'93) was born on June 26, 1966 in Timmins, Ontario, Canada. He received the B.Sc. degree in computer science and the B.E.Sc. degree in electrical engineering both in 1990 from the University of Western Ontario, London, Canada. He obtained the M.Sc.A. degree in electrical engineering in 1992 from École Polytechnique de Montréal, Montréal, Canada. During that time, he was involved in the experimental characterization and modelling of MESFET's for the design of nonlinear microwave circuits.

He is currently working toward the Ph.D. degree in electrical engineering at École Polytechnique de Montréal. His research interests include the numerical modelling of electromagnetic fields for millimeterwave and optoelectronic applications.

Ke Wu (M'87–SM'92) for photograph and biography, please see p. 1114 of this Transactions.